J Appl Electrochem (2010) 40:767–776
DOI 10.1007/s10800-009-0055-4

ORIGINAL PAPER

Electrochemical characterization of Cu dissolution and chemical mechanical polishing in ammonium hydroxide–hydrogen peroxide based slurries

R. Prasanna Venkatesh · S. Ramanathan

Received: 12 July 2009 / Accepted: 4 December 2009 / Published online: 24 December 2009

Abstract Chemical mechanical polishing (CMP) of copper in ammonium hydroxide based slurry in the presence of hydrogen peroxide was investigated. The polishing trend was found to be similar to that exhibited by other slurries containing hydrogen peroxide and various complexing agents used for Cu CMP. When the hydrogen peroxide concentration is increased, the polish rate increases, reaches a maximum and then decreases. The location and the magnitude of the maximum depend on the ammonium hydroxide concentration. The dissolution of copper in the NH_4OH–hydrogen peroxide solution was probed by potentiodynamic polarization and electrochemical impedance spectroscopy (EIS) experiments. Electrical equivalent circuit (EEC) and reaction mechanism analysis (RMA) were employed to determine the mechanistic reaction pathway of Cu dissolution in NH_4OH–hydrogen peroxide system. Based on the RMA analysis, a four step catalytic mechanism with two adsorbed intermediate species is proposed.

Keywords Copper · CMP · NH_4OH · Hydrogen peroxide · EIS

1 Introduction

Copper is widely used as an interconnect material in semiconductor industries due to its good electrical conductivity and electromigration resistance [1, 2]. Chemical mechanical polishing (CMP) is one of the key processes in the formation of copper interconnects [3, 4]. During Cu CMP process, the surface of the copper is planarized by means of both mechanical and chemical actions using a pad and slurry. A typical slurry would contain an oxidizer which modifies the copper surface by chemical action, abrasive particles which remove the modified surface by mechanical action, a complexing agent to complex the removed copper ions and prevent redeposition and additionally an inhibiting agent to minimize corrosion. A slurry must yield a reasonably high polish rate to be of use in production. It must also offer rapid self passivation of the copper surface [4].

Recently there is a renewed interest in alkaline system as CMP slurries since acidic slurries, which are widely used in Cu CMP process, may corrode the CMP equipment [5]. Investigation of Cu CMP in alkaline slurries containing ammonical compounds [2, 6–9], glycine–hydrogen peroxide mixture [10, 11] and arginine–hydrogen peroxide mixture [12] have been reported in literature. Ammonia can form complexes with copper ions. In ammonia based slurries, the etch rate was found to be low and it was reported that the copper removal was mainly mechanical [2, 4]. The low etch rate is due to the oxidation of copper by dissolved oxygen and the subsequent complexation of the cuprous ions by ammonia. Tsai et al. [13] proposed a detailed mechanism for the dissolution of copper in ammonium hydroxide in presence of dissolved oxygen. In alkaline medium, copper surface would be covered with copper oxides and hydroxides. They would reduce the etch rate but do not offer passivation and evidence of localized corrosion of copper in alkaline medium has been reported [14]. The chemical mechanical polishing efficiency factor, which is defined as the ratio of removal rate to etch rate, was found to be high in ammonical slurries [13]. However, it is necessary to enhance the removal rate [13] and offer better protection from corrosion [14].

R. Prasanna Venkatesh · S. Ramanathan (✉)
Department of Chemical Engineering, IIT-Madras,
Chennai 600036, India
e-mail: srinivar@iitm.ac.in

Various oxidizing agents such as KNO_3 [13], NH_4NO_3 [2], $NaClO_3$ [5] and K_3FeCN_6 [2] have been added to ammonical slurries and the copper polishing in these slurries have been characterized. However, these oxidizers lead only to active dissolution but not to passivation [4]. Hydrogen peroxide is a clean oxidizer that has been used for Cu CMP [10–12, 15–17]. Although in acidic pH range, the surface of copper is not passivated in presence of hydrogen peroxide [4], it is a suitable candidate as oxidizer in alkaline CMP slurries. In this work, the CMP of copper in ammonia and hydrogen peroxide based slurry is reported. The dissolution of copper in NH_4OH–hydrogen peroxide solutions is studied by potentiodynamic polarization experiments and electrochemical impedance spectroscopy (EIS). Electrical equivalent circuit (EEC) and reaction mechanism analysis (RMA) are employed to model the EIS data.

2 Experimental procedures

2.1 Copper removal experiments

The polishing experiments were carried out using a bench top LaboPol-5/LaboForce-3 polisher (Struers). Electrochemical grade copper disks of 25.4 mm diameter were used for all the polishing experiments. The slurry consisted of fumed silica abrasives (M5 cab-o-sil with the surface area of 200 $m^2\ g^{-1}$, from Cabot-Sanmar, India), NH_4OH and hydrogen peroxide. The abrasive concentration in the slurry was maintained at 2 (wt vol^{-1})%. The concentration of NH_4OH was maintained at either 0.1 or 0.05 M. The concentration of hydrogen peroxide was varied between 0 to 10 vol%. All the experiments were conducted at natural pH value of the slurries. No other chemical, such as a surfactant or a pH modifier, was added to the slurry. For slurries containing 0.1 M NH_4OH, the natural pH value varied from 10.6 (for 0% H_2O_2) to 9.2 (for 10% H_2O_2). For the slurries with 0.05 M NH_4OH, the natural pH varied from 10.4 (for 0% H_2O_2) to 8.9 (for 10% H_2O_2). For all the CMP experiments, a pressure of 5.7 psi was applied. The sample was rotated at 250 rpm and the turntable with the pad was rotated at 150 rpm. The slurry was supplied continuously using a peristaltic pump connected to the CMP tool. During polishing, the slurry was continuously stirred by a magnetic stirrer and pumped to the pad-sample interface at a flow rate of 60 mL min^{-1}. The polishing was conducted for 3 min. At least three identical runs were conducted and the average removal rates along with the standard deviations are reported in nm/min. The removal rates were calculated using weight loss method. The sample weight was measured before and after the experiment using a Sartorius balance (0.1 mg accuracy) and the difference was noted as weight loss.

2.2 Electrochemical experiments

All the chemicals are of analytical grade and MilliQ (Millipore) water was used for all the experiments. A conventional three electrode electrochemical cell connected to the PARSTAT 2263 electrochemical instrument (Princeton Applied Research) was used to carry out all the electrochemical experiments. The working electrode was a copper rod of 9 mm diameter (99.9999% purity, Aldrich) whereas the reference and counter electrodes were Ag/AgCl (3.5 M KCl) and platinum electrode (both from CH instruments) respectively. The cell was placed inside a Faraday cage to minimize interference from electrical noise. Sodium sulphate (0.1 M) was used as supporting electrolyte in all electrochemical experiments to increase the conductivity of the solution. No abrasives were used for the electrochemical experiments since the electrochemical studies here focus mainly on the chemical dissolution and passivation. Potentiodynamic polarization curves were obtained by scanning the potential at a rate of 1 mV s^{-1} from −250 to 250 mV vs. OCP. The impedance data were obtained by superimposing an ac perturbation of 10 mV (peak to peak) in the frequency range of 100 kHz–1 mHz, over the DC potential. Commercial software Zsimpwin was used to estimate the EEC parameters and sequential quadratic programming was used to estimate the RMA parameters.

3 Results and discussion

3.1 CMP experiments

Figure 1a shows the polish rate of copper vs. concentration of hydrogen peroxide in slurries containing 2% (wt vol^{-1}) silica and two different concentrations of ammonium hydroxide. Figure 1b shows the polish rate data at lower concentrations of hydrogen peroxide, expanded for clarity. In the absence of hydrogen peroxide, there is very little increase in the polish rate with increase in NH_4OH concentration. For slurry containing 0.1 M ammonium hydroxide, with the addition of hydrogen peroxide, the polish rate increases to a maximum and then starts decreasing before its value levels off at about 0.1 vol% of hydrogen peroxide. Similar trend has been reported in literature for slurry systems containing glycine–hydrogen peroxide [10, 11], arginine–hydrogen peroxide [12], phthalic acid–hydrogen peroxide [15], citric acid–hydrogen peroxide [18] and oxalic acid–hydrogen peroxide [19]. The reason that the polish rate shows a maximum at a particular

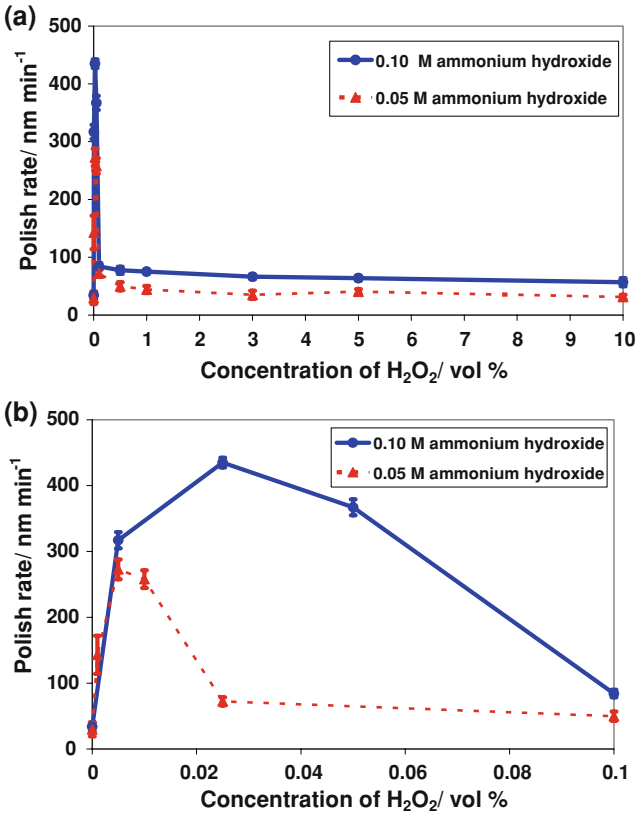

Fig. 1 **a** Polish rates of copper at various vol% of H_2O_2 containing 2 wt% silica, with 0.05 M NH_4OH and 0.1 M NH_4OH. **b** Expanded view of (**a**) at lower concentrations of H_2O_2

concentration of hydrogen peroxide is usually described as follows. At lower concentrations, hydrogen peroxide increases the oxidation state of copper thereby enhancing the polish rate of Cu. The oxidized copper would be removed by the complexing action of ammonia or any other complexing agent present in the slurry, as well as by mechanical abrasion. However, at higher concentrations of hydrogen peroxide, a thick oxide layer would be formed over the copper surface which would lead to reduced removal rates. In acidic conditions, hydrogen peroxide may not offer passivation [14] since Pourbaix diagram predicts that copper would not form stable oxide or hydroxide films at low pH [20]. In alkaline pH, there is more likelihood that the presence of hydrogen peroxide will result in the formation of oxide and/or hydroxide film on the copper surface.

The polish rate shows a maximum at 0.025 vol% of hydrogen peroxide for slurries containing 0.1 M NH_4OH and 0.005 vol% of hydrogen peroxide for slurries containing 0.05 M NH_4OH. The peak polish rate value is also lower for slurries containing the lower concentration of NH_4OH. Similar trend has been reported in the literature for glycine–hydrogen peroxide system [10, 11] where the location of the peak shifted from 2.5 wt% hydrogen peroxide for 0.1 M glycine to 0.25 wt% of hydrogen peroxide for 0.01 M glycine at a pH value of 4. The complexing ability of the slurry will increase with increasing concentration of ammonia. The exact location where the peak occurs would depend on the dynamic equilibrium between the rate of oxide formation on the copper surface and the rate of removal by chemical as well as mechanical actions. The fact that increasing ammonium hydroxide concentration leads to increased peak polish rate and that the polish rate peak occurs at a higher concentration of hydrogen peroxide supports the hypothesis proposed in the literature.

The high peak polish rate at a low concentration of hydrogen peroxide indicates that there is significant chemical dissolution in those regions. Thus it is possible to obtain high removal rates and controlled etch rates of copper in ammonium hydroxide solution if hydrogen peroxide is present. However, the entire variation in the polish rate occurs over 0.1 vol% of hydrogen peroxide concentration for slurries containing 0.1 M NH_4OH. Figure 1b shows that the variation is even more rapid for slurries with 0.05 M NH_4OH. The rate of change in copper polish rate depends on the concentration and complexing ability of the ammonium species as well as the kinetics of copper ion formation. The rapid variation in removal rate would make the CMP process difficult to control. Literature shows that copper CMP removal rate varied between about 140 to about 40 nm/min over a concentration range of 5% of hydrogen peroxide in solutions containing 0.01 M glycine maintained at pH 4 [10]. At a pH value of 9, the removal rate varied between about 100 nm/min to about 50 nm/min over the same concentration range of hydrogen peroxide. Thus the complexing ability may be enhanced by adjusting the pH and by adding suitable ammonium salts. Copper dissolution in solutions containing hydrogen peroxide and citric acid has been studied and it exhibits a maximum with respect to hydrogen peroxide concentration [18]. The rate of change of dissolution rate also depends on the rotation of the copper sample. Thus mechanical parameters such as the speed of rotation and pressure may also play a role. Moreover, mechanical removal action has been shown to increase the dissolution of copper in glycine-hydrogen peroxide solutions [10]. Further investigations with patterned wafers are necessary to optimize the slurry composition for all the performance parameters such as polish rate variation, uniformity, roughness, dishing and erosion. A higher ammonium concentration to enhance the complexation, a suitable corrosion inhibitor, optimal pH value, using abrasives of different hardness values and slurries with various solids concentrations and modified polishing conditions such as pressure, velocity etc. may be necessary to obtain robust polish rates and minimum dissolution rates.

3.2 Electrochemical measurements

3.2.1 Potentiodynamic polarization studies

Figure 2a and b show the potentiodynamic polarization curves for 0.1 M NH_4OH at various concentration of peroxide with 0.1 M Na_2SO_4 as supporting electrolyte. Sodium based solutions can not be used for actual semiconductor processing due to contamination issues. However, in order to understand the electrochemical aspects of metal dissolution in slurry chemicals, salts such as Na_2SO_4, $NaNO_3$ and $NaClO_3$ have been used as supporting electrolytes to reduce the solution resistivity [10, 14, 21–24]. A kink was observed in the anodic branch of the plot for solutions containing hydrogen peroxide concentration of less than 0.5%. If the hydrogen peroxide concentration is equal to or more than 0.5%, the kink disappears. The appearance of kink in the anodic branch of the potentiodynamic polarization plot is probably due to the formation of oxides and hydroxides over the copper surface [14, 20, 21, 25, 26].The oxide and hydroxide layers could cause a decrease in the anodic current without offering passivation.

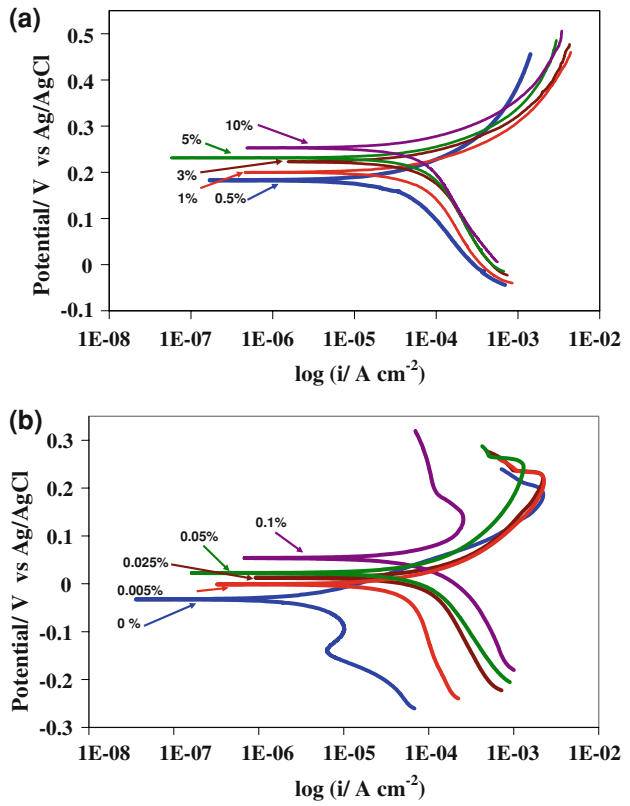

Fig. 2 Potentiodynamic polarization curves of copper in solutions containing 0.1 M NH_4OH and 0.1 M Na_2SO_4 and various vol% of H_2O_2. Percentage values mentioned inside the figure indicates concentration of H_2O_2. **a** Higher H_2O_2 concentrations, **b** lower H_2O_2 concentrations

The values of E_{corr} and I_{corr} were determined by extrapolating anodic and cathodic branch of the potentiodynamic polarization plot by using the software Powercorr. The values of both I_{corr} and E_{corr} are shown in the Fig. 3. At low hydrogen peroxide concentrations, there is a limited region exhibiting Tafel like behavior and hence the inaccuracy in the estimate of I_{corr} value would be higher. The value of E_{corr} increases with the hydrogen peroxide concentration and this is similar to the behavior reported for copper electrode in peroxide and other complexing agents [10, 11, 18, 26].On the other hand, the I_{corr} value reaches a maximum corresponding to 0.1 vol% hydrogen peroxide concentrations. Further increase in hydrogen peroxide concentration leads to a decrease in I_{corr}, even though there is no kink in the anodic branch of the polarization curve. This trend is also seen with copper dissolving in solutions containing hydrogen peroxide and amino acids such as glycine and arginine [11, 12, 26]. In the presence of H_2O_2, in addition to Cu redox reactions, H_2O_2 redox reactions would also occur [10]. The H_2O_2 redox reaction would be more dominant, especially at higher H_2O_2 concentrations. For Cu dissolving in solutions containing glycine and H_2O_2, a similar trend has been observed viz. the polish rates and dissolution rates show a maximum when the H_2O_2 concentration was increased, but the anodic polarization curves did not show any kink. The current contributions from H_2O_2 oxidation reactions might have over shadowed the copper redox reactions in the polarization curves, which result in the disappearance of kink in the anodic branch. Similarly, even though Cu dissolution was low in those solutions at high H_2O_2 concentrations, it was higher than that in solutions without H_2O_2 [10]. Thus, complete passivation does not occur at high concentrations of H_2O_2 and the dissolution is active at the higher potentials. The variation of I_{corr} with hydrogen peroxide concentration is similar to that of the variation of CMP

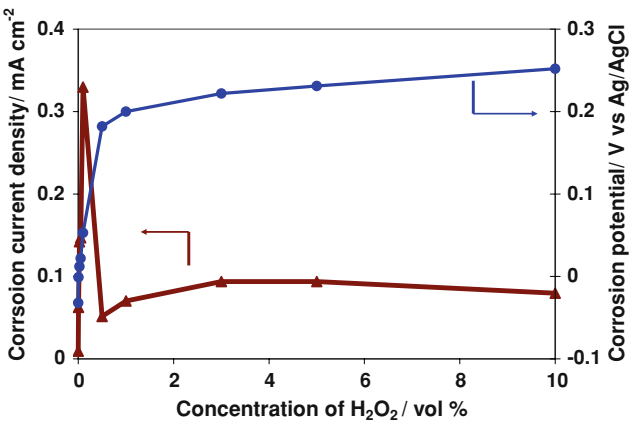

Fig. 3 The values of I_{corr} and E_{corr} for copper on solutions containing 0.1 M NH_4OH and 0. 1 M Na_2SO_4 and various vol% H_2O_2

removal rate indicating that, unlike pure ammonium hydroxide slurries, chemical dissolution also contributes to the overall removal in CMP in these slurries. This comparison is only qualitative since the CMP involves mechanical and chemical actions, while the dissolution experiments measure only the chemical component.

3.2.2 EIS measurements

EIS is an important tool in understanding electrode characteristics and electrochemical reactions at the electrode interface [27]. Since the variation in polish rate at lower H_2O_2 concentrations is rapid and polish rate is more stable at higher H_2O_2 concentrations, the EIS experiments were carried out at 1% H_2O_2. EIS study was carried out for copper electrode in 0.1 M NH_4OH and 1 vol% hydrogen peroxide concentration with 0.1 M Na_2SO_4 as supporting electrolyte. The impedance spectra at various anodic potentials can be employed to elucidate the kinetics of metal dissolution [22, 23, 28–36]. The OCP value of the copper in 0.1 M NH_4OH–1 vol% hydrogen peroxide system is 200 mV vs. Ag/AgCl and hence the EIS data was acquired at anodic potentials with an interval of 50 mV starting at the OCP. For an electrochemical system which is stable and responds linearly to the applied ac perturbation, the EIS data will obey Kramers–Kronig Transform (KKT) [27]. If the imaginary part of the EIS spectra is known for the complete frequency range (zero to infinity), the real part can be estimated by the KKT and vice versa. Practically, if the data is measured over a wide frequency range, the KKT can be applied to the data. While satisfying KKT is a necessary condition for the stability and linearity of the electrochemical system, it is not a sufficient condition [27]. Nevertheless, it is used to validate the EIS data before subjecting the data to linear analysis such as EEC or RMA. In the present work, EIS measurements were acquired in the active dissolution region and for a duration of about 50 min. The data was validated by KKT before proceeding with further analysis. For NH_4OH–H_2O_2 system, for most of the potentials, the transformed data overlaps with the raw data. Only at the highest anodic potential investigated (350 mV) and at the low frequency range, the experimental and transformed values of real part of impedance show variation as high as 12%. Considering that the dissolution is higher at that potential and that the low frequency data takes about 17 min, this is not surprising. For all other frequencies and overpotentials, the data quality is very good. Figure 4 shows the data in Nyquist format for above mentioned system at various DC potentials. It is seen that there are two capacitance loops at all the overpotentials. The total impedance decreases with an increase in DC potential, which indicates that the dissolution rate is higher at higher potential. The high

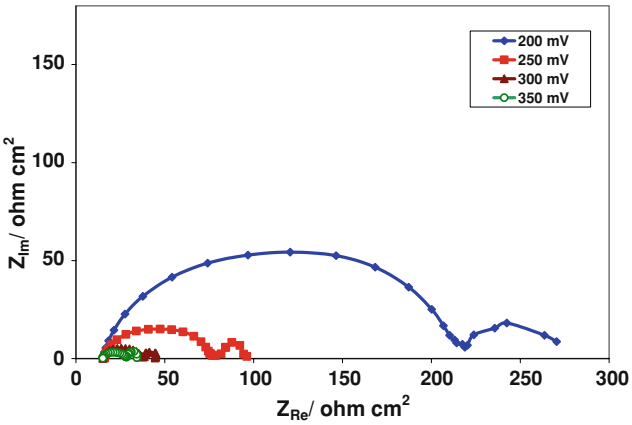

Fig. 4 Experimental EIS data at various overpotentials for copper in 1 vol% H_2O_2, 0.1 M NH_4OH and 0. 1 M Na_2SO_4

frequency loop is a depressed semicircle indicating that a constant phase element (CPE), rather than a simple capacitor, would represent the electrode solution interface better. The experimental EIS data was modeled by EEC and RMA in order to elucidate the dissolution mechanism.

3.2.3 EEC model fitting

An EEC comprising of electrical components such as resistors, capacitors and inductors can be used to model the experimental EIS data. This would facilitate an understanding of the electrochemical reaction process [34]. The model used to fit the experimental EIS data is shown in Fig. 5. A similar circuit has been applied to fit the EIS data of copper dissolving in arginine–hydrogen peroxide solution [22]. Here R_{soln} is the solution resistance and Q represents the constant phase element (CPE) which is modeled by two parameters Y_o and n. The resistance R_2 is associated with the Faradaic reactions whereas R_1 and C_1 are resistance and capacitance associated with the non Faradaic reactions. Figure 6 shows the EEC model fit to the experimental data along with the RMA estimates discussed below. The parameters obtained from this EEC fit are summarized in the Table 1. It is clear from Fig. 6 that the circuit model captures the essential features of experimental data well at all the overpotentials. Table 1 shows

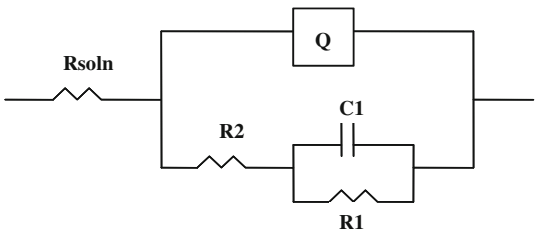

Fig. 5 Electrical equivalent circuit for copper in 1 vol% H_2O_2, 0.1 M NH_4OH and 0. 1 M Na_2SO_4

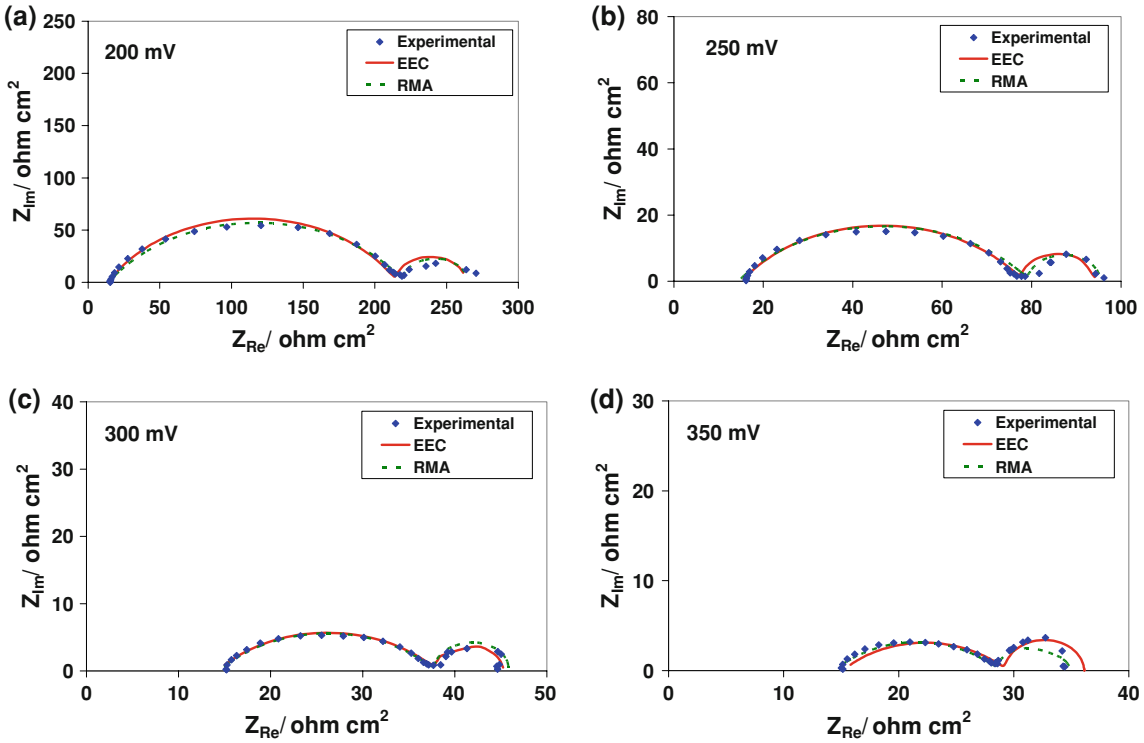

Fig. 6 Best fit EIS values superimposed with experimental data at **a** 200 mV **b** 250mV **c** 300 mV and **d** 350 mV (vs. Ag/AgCl) for copper in 1 vol% H_2O_2, 0.1 M NH_4OH and 0.1 M Na_2SO_4. Both electrical equivalent circuit (EEC) best fit results and the reaction mechanism analysis (RMA) best fit results are shown

Table 1 EEC parameters obtained at various overpotentials for copper electrode in 1 vol% hydrogen peroxide, 0.1 M NH_4OH and 0.1 M Na_2SO_4

Potential/mV vs. Ag/AgCl	Y_o/Ω^{-1} cm^{-2} S^n	n	R_1/Ω cm^2	C_1/F cm^{-2}	R_2/Ω cm^2
200	1.21×10^{-4}	0.69	48.04	0.633	201.09
250	2.85×10^{-4}	0.63	9.78	0.708	54.88
300	6.28×10^{-4}	0.56	7.16	0.772	24.24
350	1.03×10^{-3}	0.52	6.4	0.813	14.28

that R_1 decreases with overpotential while C_1 increases with overpotential. Since both R_1 and C_1 are associated with the same reaction, it shows mutually opposing trends [22, 23]. R_2 decreases with an increase in potential, indicating that the rate of Faradaic reaction is higher at higher potentials. The value of n of the CPE decreases with overpotential. For an ideal capacitor, the value of n would be 1 and a rough electrode would lead to slightly lower value of n. On the other hand, a dominance of diffusion effects would results in a value of 0.5 for n, which represents Warburg impedance. At higher overpotentials, when the dissolution rate is high, the dissolved Cu ions will accumulate near the surface. The diffusion of these Cu ions into the bulk solution may became the rate limiting step. The fact that the value of n is low and is decreasing with an increase in potential indicates that the electrode roughness was increasing with overpotential and also that the diffusion effects are dominant [22].

3.2.4 *Reaction mechanism analysis*

The dissolution of copper in acidic medium has been studied extensively for a wide range of pH and overpotentials [37, 38]. The following two step mechanism has been proposed for copper dissolution in acidic media at lower overpotentials [37].

$$Cu \rightleftharpoons Cu^{+}_{ads} + e^{-} \quad (1)$$

$$Cu^{+}_{ads} \rightarrow Cu^{2+} + e^{-} \quad (2)$$

At higher overpotentials, the following additional steps involving autocatalytic mechanism have been proposed [38].

$$Cu^{+}_{ads} \rightleftharpoons Cu^{2+}_{ads} + e^{-} \quad (3)$$

$$Cu^{2+}_{ads} + Cu \rightarrow Cu^{2+} + Cu^{2+}_{ads} + 2e^{-} \quad (4)$$

In acidic media, there will not be a stable protective film on the copper surface. However in alkaline medium, oxide and hydroxide layers are expected to be present on the copper surface and various electrochemical and non- electrochemical techniques has been employed to investigate the nature of the films and the kinetics of film formation [25, 39–42]. A few systems with hydrogen peroxide and complexing agent in alkaline environment has been investigated [10, 12, 22]. Here the mechanistic reaction pathway of copper dissolution in solution containing NH_4OH and hydrogen peroxide is determined by RMA of the EIS data.

The following direct dissolution mechanism leads to a single capacitance loop [22].

$$Cu \xrightarrow{k_1} Cu^{2+} + 2e^{-} \quad (5)$$

where k_1 is the rate constant of reaction step 1 and is given by $k_1 = k_{10}e^{b_1 V}$. Here k_{10} is the pre-exponential factor and b_1 is the exponent. Since the impedance data of the present system exhibits two capacitance loops, the direct dissolution step is ruled out. Five different mechanisms, shown in Table 2, were used to model the EIS data. All of them resulted in two capacitance loops at all overpotentials. While it would be tempting to fit the data to simpler model, minimizing the number of parameters in a model should not be the sole criteria for choosing a model. The main objective is to use the model to learn about the processes in the system [27]. Mechanism 1, which has been proposed for modeling dissolution of copper in arginine–hydrogen peroxide solution [22], did not fit the experimental data adequately, especially at higher potentials. Mechanism 2 is similar to mechanism 1 with an additional reverse step. Although the fit was better with mechanism 2 than with mechanism 1, the essential features were not captured well. Mechanism 3 has been proposed for modeling the dissolution of copper in glycine–hydrogen peroxide system [23] and mechanism 4 is similar to mechanism 3 with an additional reverse step. However, the model fit results are not significantly better. Catalytic mechanisms have been proposed for modeling copper dissolution in acidic system [38, 43] as well as other metal dissolution [30, 31]. In mechanism 5, the final step is the reaction between Cu^{2+*}_{ads} species and Cu. In this second order reaction, the dissolution of Cu needs the presence of Cu^{2+*}_{ads} species and the Cu^{2+*}_{ads} species is regenerated. Hence this mechanism is referred to as catalytic mechanism in the literature. The derivation of impedance equations for various mechanisms has been reported [30–32] and only the derivation for proposed catalytic mechanism is summarized below.

Table 2 Various mechanisms that were employed to model copper dissolution in 0.1 M NH_4OH–0.1 M Na_2SO_4–1 vol% hydrogen peroxide

Mechanism	Equation
Mechanism 1	$Cu \xrightarrow{k_1} Cu^{2+}_{ads} + 2e^{-} \xrightarrow{k_2} Cu^{2+}_{sol}$
Mechanism 2	$Cu \underset{k_{-1}}{\overset{k_1}{\rightleftharpoons}} Cu^{2+}_{ads} + 2e^{-} \xrightarrow{k_2} Cu^{2+}_{sol}$
Mechanism 3	$2Cu + H_2O_2 \xrightarrow{k_1} Cu_2O$
	$Cu_2O + H_2O \xrightarrow{k_2} 2CuO + 2H^{+} + 2e^{-}$
	$CuO + 2NH_4^{+} \xrightarrow{k_3} [Cu(NH_3)_2]^{2+} + H_2O$
Mechanism 4	$2Cu + H_2O_2 \underset{k_{-1}}{\overset{k_1}{\rightleftharpoons}} Cu_2O$
	$Cu_2O + H_2O \xrightarrow{k_2} 2CuO + 2H^{+} + 2e^{-}$
	$CuO + 2NH_4^{+} \xrightarrow{k_3} [Cu(NH_3)_2]^{2+} + H_2O$
Mechanism 5	$Cu \underset{k_{-1}}{\overset{k_1}{\rightleftharpoons}} Cu^{2+}_{ads} + 2e^{-}$
	$Cu^{2+}_{ads} \xrightarrow{k_2} Cu^{2+}_{sol}$
	$Cu^{2+}_{ads} \underset{k_{-3}}{\overset{k_3}{\rightleftharpoons}} Cu^{2+*}_{ads}$
	$Cu^{2+*}_{ads} + Cu \xrightarrow{k_4} Cu^{2+}_{sol} + Cu^{2+*}_{ads} + 2e^{-}$

For the catalytic mechanism 5, the unsteady state mass balance equations for adsorbed species can be written as

$$\tau\frac{d\theta_1}{dt} = k_1(1-\theta_1-\theta_2) - k_{-1}\theta_1 - k_2\theta_1 - k_3\theta_1 + k_{-3}\theta_2 \quad (6)$$

$$\tau\frac{d\theta_2}{dt} = k_3\theta_1 - k_{-3}\theta_2 \quad (7)$$

where τ is the total number of sites for the given electrode surface and θ_1 and θ_2 is the surface coverage of the adsorbed species of Cu^{2+}_{ads} and Cu^{2+*}_{ads} respectively. Under steady state conditions, the surface coverage will be

$$\theta_{1ss} = \frac{k_1}{(k_1 + k_{-1} + k_2 + k_3) + (k_3/k_{-3})(k_1 - k_{-3})} \quad (8)$$

$$\theta_{2ss} = \frac{k_3}{k_{-3}}\theta_{1ss} \quad (9)$$

The current due to Faradaic reaction is given below

$$J = 2F[k_1(1-\theta_1-\theta_2) - k_{-1}\theta_1 + k_4\theta_2(1-\theta_1-\theta_2)] \quad (10)$$

where F is the Faraday constant. The Faradaic impedance $(Z_{F,m/s})$ is obtained by taking the derivative of above equation with respect to the voltage and is given by

$$(Z_{F,m/s})^{-1} = \frac{dJ}{dV} = (R_t)^{-1} - 2F(k_1 + k_{-1} + k_4\theta_{2ss})\frac{d\theta_1}{dV} - 2F(k_1 - k_4 + 2k_4\,\theta_{2ss} + k_4\theta_{1ss})\frac{d\theta_2}{dV} \quad (11)$$

where

$$(R_t)^{-1} = 2F[b_1k_1(1 - \theta_{1ss} - \theta_{2ss}) - b_{-1}k_{-1}\theta_{1ss} + b_4k_4\,\theta_{2ss}(1 - \theta_{1ss} - \theta_{2ss})] \quad (12)$$

$$\frac{d\theta_1}{dV} = \frac{CE - BF}{AE - BD} \quad (13)$$

$$\frac{d\theta_2}{dV} = \frac{F - D\frac{d\theta_1}{dV}}{E} \quad (14)$$

Here

$$A = k_1 + k_{-1} + k_2 + k_3 + j\omega\tau \quad (15)$$

$$B = k_1 - k_{-3} \quad (16)$$

$$C = b1k1 - (b_1k_1 + b_{-1}k_{-1} + b_2k_2 + b_3k_3)\,\theta_{1ss} - (b_1k_1 - b_{-3}k_{-3})\,\theta_{2ss} \quad (17)$$

$$D = -k_3 \quad (18)$$

$$E = k_{-3} + j\omega\tau \quad (19)$$

$$F = (b_3 - b_{-3})\,k_3\,\theta_{1ss} \quad (20)$$

R_t represents the resistance to charge transfer. The equation for total impedance is given below

$$Z_{\text{Total}} = R_{\text{sol}} + \frac{1}{Y_0(j\omega)^n + (Z_{F,m/s})^{-1}} \quad (21)$$

Here Y_o represents the parameter of CPE and n represents the exponent for CPE. Figure 5 shows the best fit RMA estimates along with the experimental EIS data. The parameter set, which minimizes the following residue term, is given in Table 3.

$$\text{residue} = \sum \left[w_{\text{Re}}\left(\text{Z}_{\text{Re}_{\text{experimental}}} - \text{Z}_{\text{Re}_{\text{bestfit}}}\right)^2 + w_{\text{Im}}\left(\text{Z}_{\text{Im}_{\text{experimental}}} - \text{Z}_{\text{Im}_{\text{bestfit}}}\right)^2\right] \quad (22)$$

The residue is taken over all the frequencies and overpotentials. Here w_{Re} and w_{Im} are the weighing functions which can be chosen as unity or as the inverse of value of real and imaginary parts [27]. If the impedance values span over an order of magnitude or more, the chosen of weight may make a significant difference in optimized parameter set. However, in this case, the parameter values were not very sensitive to the weight function and the parameter set given in the Table 3 is based on unity weight function. The best fit RMA plots are shown in Fig. 6.

The catalytic mechanism captures all the experimental data well at all overpotentials. Specifically, the total impedance decreases with overpotential and both the capacitance loop at high and low frequency regimes shrink with an increase in potential. The residues obtained with various mechanisms are summarized in Table 4. Since the number of parameters used to fit the data changes with the choice of model, a direct comparison between the residues is not appropriate. In order to confirm that the catalytic mechanism is indeed the appropriate choice, Akakie Information Criterion (AIC) was applied to the residues [44]. The expression for calculating AIC is given below.

$$\text{AIC} = 2\,k + n\left[\ln\left(\frac{\text{residue}}{n}\right)\right] \quad (23)$$

where n is the total number of observations and k is the total number of independently adjusted parameters in the given model. An increase in the number of parameters would increase the penalty in the AIC. The AIC values

Table 3 Best fit parameters used for RMA

k parameter	Value	Units
k_{10}	1.09×10^{-9}	mol cm^{-2} s^{-1}
b_1	25.26	V^{-1}
k_{-10}	2.03×10^{-9}	mol cm^{-2} s^{-1}
b_{-1}	0	V^{-1}
k_{20}	9.06×10^{-9}	mol cm^{-2} s^{-1}
b_2	8.81	V^{-1}
k_{30}	1.88×10^{-10}	mol cm^{-2} s^{-1}
b_3	16.35	V^{-1}
k_{-30}	1.56×10^{-8}	mol cm^{-2} s^{-1}
b_{-3}	−2.54	V^{-1}
k_{40}	4.69×10^{-9}	mol cm^{-2} s^{-1}
b_4	17.87	V^{-1}
Y_o at 200 mV	1.72×10^{-4}	Ω^{-1} cm^{-2} S^n
n at 200 mV	0.64	
Y_o at 250 mV	3.28×10^{-4}	Ω^{-1} cm^{-2} S^n
n at 250 mV	0.60	
Y_o at 300 mV	6.25×10^{-4}	Ω^{-1} cm^{-2} S^n
n at 300 mV	0.57	
Y_o at 350 mV	9.06×10^{-4}	Ω^{-1} cm^{-2} S^n
n at 350 mV	0.55	
τ	3.61×10^{-7}	mol cm^{-2}
R_{sol}	14.4	Ω cm^2

Table 4 Residues obtained for various mechanisms

Mechanism	No. parameters	Residue	AIC
Mechanism 1	14	2525	366
Mechanism 2	16	2160	379
Mechanism 3	16	2333	388
Mechanism 4	18	2333	392
Mechanism 5	22	1119	312

obtained with various mechanisms are also summarized in Table 4. The model which has the minimum AIC value is chosen as the best fit. Mechanism 5 has the minimum AIC and hence it is taken as appropriate model to describe copper dissolution in the NH_4OH–hydrogen peroxide system. From Table 4, it is clear that the values of n and Y_o associated with the CPE follow the same trend as EEC model estimates. The values of pre-exponents and the exponents associated with the rate constants compare well with those reported in literature for other metal dissolution reactions [22, 30, 45, 46]. The fact that a more detailed mechanism is needed to model the experimental data adequately, even though a simple electrical equivalent circuit captures the features well indicates that the EEC can mainly offer guidance about the behavior of the electrochemical reactions and not necessarily the details of the mechanistic pathway. The proposed mechanism indicates that the copper surface is covered with cupric oxides in the solution at the potentials under investigations. In situ electrochemical characterization is in progress to understand the system better. The actual composition of the surface has to be confirmed by other techniques such as spectroscopy or electrochemical scanning tunneling microscopy to obtain a more thorough understanding of the interfacial reactions.

4 Conclusions

Copper CMP in slurries containing hydrogen peroxide and ammonium hydroxide was characterized and it was found that the polish rate shows a maximum at 0.025 and 0.005 vol% of hydrogen peroxide concentration for 0.1 M NH_4OH and 0.05 M NH_4OH respectively. The chemical removal component of the total removal is enhanced by addition of suitable quantity of hydrogen peroxide. The corrosion current also shows similar behavior with increase in hydrogen peroxide concentration. Potentiodynamic polarization experiments show that at low concentrations of hydrogen peroxide, a kink is observed in the anodic branch of the plot while at higher concentrations the kink disappears. EIS data show two capacitance loops at all the over potentials. Electrical equivalent circuit analysis and reaction mechanism analysis were employed to analyze the EIS data. A four step catalytic mechanism with two adsorbed intermediate species is proposed for Cu dissolution in NH_4OH–hydrogen peroxide system. Both EEC and RMA capture the essential features of the experimental EIS data.

Although the polish rate can be modified with addition of hydrogen peroxide to ammonical slurries, the rapid variation in polish rate indicates that the slurry needs to be optimized further. Optimization with respect to concentration of neutral and charged ammonium species, the pH value, abrasive type and contents, polishing conditions such as pressure, velocity and pad type are necessary to obtain robust polish rates and uniformity as well to minimize the dishing and erosion. The surface of copper in ammonium hydroxide and hydrogen peroxide solution also needs to be analyzed by complimentary technique such as electrochemical tunneling microscopy and spectroscopy to understand the interfacial processes better and verify the findings of EIS.

Acknowledgments The authors would like to thank Prof. Digby D. Macdonald, Department of Materials Science and Engineering, Pennsylvania State University, (macdonald@matse.psu.edu) for the Kramers–Kronig Transformation software.

References

1. Nitta T, Ohmi T, Hoshi T et al (1993) J Electrochem Soc 140:1131
2. Steigerwald JM, Murarka SP, Gutmann RJ et al (1995) Mater Chem Phys 41:217
3. Steigerwald JM, Murarka SP, Gutmann RJ (1997) Chemical mechanical planarization of microelectronic materials. Wiley, Newyork
4. Oliver MR (2004) In: Oliver MR (ed) Chemical-mechanical planarization of semiconductor materials. Springer, Berlin
5. Luo D, Campbell DR, Babu SV (1997) Thin Solid Films 311:177
6. Steigerwald JM, Duquette DJ, Murarka SP et al (1995) J Electrochem Soc 142:2379
7. Sainio CA, Duquette DJ, Murarka SP et al (1996) J Electrochem Soc 25:1593
8. Osseo-Asare K, Mishra KK (1996) J Electron Mater 25:1599
9. Carpio R, Farkas J, Jairath R (1995) Thin Solid Films 266:238
10. Aksu S, Wang L, Doyle FM (2003) J Electrochem Soc 150:G718
11. Seal S, Kuiry SC, Heinmen B (2003) Thin Solid Films 423:243
12. Nagendra Prasad Y, Ramanathan S (2007) Electrochim Acta 52:6353
13. Tsai T-H, Yen S-C (2003) Appl Surf Sci 210:190
14. Ein-Eli Y, Abelev E, Rabkin E et al (2003) J Electrochem Soc 150:C646
15. Hernandez J, Wrschka P, Oehrlein GS (2001) J Electrochem Soc 148:G389
16. Hirabayashi H, Higuchi M, Kintoshita M et al (1996) In: Proceedings of the second international CMP for ULSI multilevel interconnects conference (CMP–MIC), p 119
17. Paul E, Kaufman F, Brusic V et al (2005) J Electrochem Soc 152:G867
18. Chen JC, Lin S-R, Tsai W-T (2004) Appl Surf Sci 233:80
19. Pandija S, Roy D, Babu SV (2007) Mater Chem Phys 102:144
20. Pourbaix M (1974) Atlas of electrochemical equilibria in aqeous solutions, 2nd edn. NACE, Houston
21. Luo Q, Mackay RA, Babu SV (1997) Chem Mater 9:2101
22. Nagendra Prasad Y, Vinod kumar V, Ramanathan S (2009) J Solid State Electrochem 13:1351
23. Lu J, Garland JE, Pettit CM et al (2004) J Electrochem Soc 151:G717
24. Carter MK, Small RJ (2003) J Electrochem Soc 150:G107
25. Strehblow HH, Titze B (1980) Electrochim Acta 25:839
26. Du T, Vijayakumar A, Desai V (2004) Electrochim Acta 49:4505

27. Macdonald JR (2005) In: Barsoukov E, Macdonald J (eds) Impedance spectroscopy, 2nd edn. Wiley, NJ
28. Sapra S, Li H, Wang Z et al (2005) J Electrochem Soc 152B:193
29. Schweickert CH, Lorenz WJ, Friedburg H (1980) J Electrochem Soc 127:1693
30. Keddam M, Mattos OR, Takenouti H (1981) J Electrochem Soc 128:257
31. Bojinov M (1996) J Electronal Chem 405:15
32. Gregori J, Gimenex-Romero D, Garcia-Jareno JJ et al (2006) J Solid State Electrochem 10:920
33. Macdonald DD, Real S, Smedley SI et al (1988) J Electrochem Soc 138:2410
34. Harrington DA, Van den Driessche P (2004) J Electronal Chem 567:153
35. Folquer ME, Ribotta SB, Real SG et al (2002) Corrossion 58:240
36. Diard JP, Le Canut JM, Le Correc B et al (1988) Electrochim Acta 43:2485
37. Bockris JO'M, Enyo M (1962) Trans Farday Soc 58:1187
38. Cordeiro CGO, Barcia OE, Mattos OR (1993) Electrochim Acta 38:319
39. Lohrengel MM, Schultze JW, Speckmann HD et al (1987) Electrochim Acta 32:733
40. Gomez Becerra J, Salvarezza RC, Arvia AJ (1988) Electrochim Acta 33:613
41. Maurice V, Strehblow HH, Marcus P (2000) Surf Sci 458:185
42. Perez Sanchez M, Barrera M, Gonzalez S et al (1990) Electrochim Acta 35:1337
43. Wong DKY, Bruce A, Coller W et al (1993) Electrochim Acta 38:2121
44. Akaike H (1974) IEEE Trans Automat Contr 19:716
45. Baril G, Galicia G, Deslouis C et al (2007) J Electrochem Soc 154:C108
46. Gregori J, Garcia-Jareno JJ, Gimenez-Romero D et al (2007) J Electrochem Soc 154:C371